



## City Research Online

### City, University of London Institutional Repository

---

**Citation:** Fonseca, J., O'Sullivan, C., Coop, M. R. & Lee, P. D. (2012). Non-invasive characterization of particle morphology of natural sands. *Soils and Foundations*, 52(4), pp. 712-722. doi: 10.1016/j.sandf.2012.07.011

This is the accepted version of the paper.

This version of the publication may differ from the final published version.

---

**Permanent repository link:** <https://openaccess.city.ac.uk/id/eprint/3533/>

**Link to published version:** <https://doi.org/10.1016/j.sandf.2012.07.011>

**Copyright:** City Research Online aims to make research outputs of City, University of London available to a wider audience. Copyright and Moral Rights remain with the author(s) and/or copyright holders. URLs from City Research Online may be freely distributed and linked to.

**Reuse:** Copies of full items can be used for personal research or study, educational, or not-for-profit purposes without prior permission or charge. Provided that the authors, title and full bibliographic details are credited, a hyperlink and/or URL is given for the original metadata page and the content is not changed in any way.

---

---

---

City Research Online:

<http://openaccess.city.ac.uk/>

[publications@city.ac.uk](mailto:publications@city.ac.uk)

---

# Non-invasive characterisation of particle morphology of natural sands

Fonseca, J.<sup>1</sup>, O'Sullivan, C.<sup>2</sup>, Coop, M.R.<sup>3</sup>, Lee, P.D.<sup>4</sup>

## Abstract

Particle morphologies, i.e. particle sizes and shapes, have a marked influence on the mechanical response of granular materials including soils. Up until now most investigations of particle shape have been two-dimensional and size has been most often assessed using sieving. This paper makes use of recent developments in three-dimensional imaging technologies to characterize the internal features of a soil in 3D including quantification of particle morphology. The soil investigated was Reigate sand (from Southeast England), a geologically old sand which, in its intact state exhibits significant interlocking amongst the constituent grains. Intact and reconstituted specimens having similar densities were tested under triaxial compression. The specimens were impregnated with an epoxy resin at three different stages of shear deformation and small cores from each specimen were scanned using X-ray micro-tomography. Different systems and scanning parameters were explored in order to obtain three-dimensional, high-resolution, images with a voxel size of  $5\mu\text{m}$  ( $0.018 \times d_{50}$ ). The morphology measurements were compared with sieve data and measurements obtained using a 2D, image based, laser system. The sieve size is shown to correlate well with the intermediate principal axis length. Clear differences are noted between the 2D and 3D shape measurements. Breakage of fractured grains, along existing fissures, occurs both during reconstitution and shearing of the intact soil, a phenomenon that cannot be observed using invasive techniques such as sieve analysis.

**Key words:** fabric/structure of soils; morphology; 3D microscopy; dilatancy; shearing; locked sand

IGS: B00, D00, D01, D03, D06

1. Dept. of Materials, Imperial College London, UK, [joana.fonseca04@imperial.ac.uk](mailto:joana.fonseca04@imperial.ac.uk)
2. Dept. of Civil Engineering, Imperial College London, UK, [cath.osullivan@imperial.ac.uk](mailto:cath.osullivan@imperial.ac.uk)
3. Dept. of Civil and Architectural Engineering, City University, Hong Kong, [mrcoop@cityu.edu.hk](mailto:mrcoop@cityu.edu.hk)
4. School of Materials, The University of Manchester, UK, [peter.lee@manchester.ac.uk](mailto:peter.lee@manchester.ac.uk)

## INTRODUCTION

The distribution of particle sizes and the grain shapes are fundamental characteristics of a soil. The particle size distribution (PSD) influences the range of attainable void ratios (e.g. Miura et al., 1997). The distribution of particle sizes influences the soil response, for example at the same relative density a better graded soil may have a larger angle of internal friction (e.g. Holtz and Kovacs, 1981). There is evidence that the PSD influences the compressibility of granular soils (e.g. Yamamuro and Wood (2004)). The particle size distribution also determines the susceptibility of soils to internal erosion (e.g. Kenney and Lau, 1985; Kezdi, 1969). Typically in geomechanics, particle size distribution is determined using sieving, but other methods are available including laser-based methods and two-dimensional image analysis based approaches (White, 2003; Cavarretta, 2009).

The influence of particle shape on the engineering properties of granular soils is widely reported in the literature. Santamarina and Cho (2004) highlighted influence of particle sphericity on the evolution of stress-induced anisotropy and showed that angularity and roughness influence both the small-strain stiffness and the large strain strength. Guo and Su (2007), amongst others, demonstrated that angularity influences the shear resistance and dilatancy properties of sands. Clayton et al. (2006) highlighted the effect of particle geometry on sand response in cyclic triaxial testing. Using DEM, Rothenburg and Bathurst (1992) showed that circular-shaped particles have much lower strengths than elliptical particles. Particle shape clearly influences the geometry of inter-particle contacts and consequently the distribution of the stresses at the contact. In the case of disks and spheres, excessive rotation can occur because the branch vector joining the centroids of two contacting particles and the contact normal are collinear. For ellipses and ellipsoids (and any natural soil particle) the branch vector and contact normal are not collinear, increasing rotational resistance. Additionally non-convex particles are more likely to develop a greater number of contacts per particle and hence exhibit higher strength and stiffness in comparison with convex particles (e.g. O'Sullivan, 2011).

The experimental tools commonly used to measure particle size distribution (i.e. sieve analysis and laser instruments) rely on invasive measures in which the initial fabric is destroyed. Recent developments in three-dimensional imaging technologies, such as X-ray micro-computed tomography (micro-CT), have enabled the investigation of the internal features of real sand specimens with a level of detail previously observed in 2D images from thin sections. Early studies using CT in granular soils considered the development of deformations (e.g. Desrues et al., 1996) and the spatial resolution used was greater than one millimetre and hence did not resolve the particles. It was not until very recently that imaging at a particle scale, i.e. of a few microns, started to be used (e.g. Bauer et al., 2004, Al-Raoush, 2007; Hasan and Alshibli, 2010; Hall et al., 2010).

This paper demonstrates the use of micro-CT data to characterize the particle morphology of sand by comparing intact and reconstituted samples of a locked sand. After outlining the experimental approach

adopted, the techniques used to analyze the micro-CT images and quantify the particle morphology are described. Then the particle size distributions (PSDs) obtained from the micro-CT images are compared with sieving and other size characterization approaches. The PSDs of the intact and reconstituted sand specimens are compared and the evolution of the PSDs during shearing is considered. The particle shapes are also compared. For the reconstituted material the 3D measures of shape are compared with 2D characterization using a laser-based image analysis approach.

## EXPERIMENTAL METHOD

### *Material description*

The Reigate sand analysed in this study forms part of the Folkestone Beds Formation (Lower Greensand). The samples were retrieved from a quarry near Reigate (Southeast England) where this geological formation outcrops. Cresswell and Powrie (2004) performed extensive laboratory investigations of its behaviour. Owing to the very high density and the interlocked fabric that the sand presents in its intact state, Reigate sand has been classified as a “locked sand” meeting the criteria proposed by Dusseault and Morgenstern (1979). Typically it is very difficult to obtain intact or undisturbed samples of a naturally deposited sand, but because of its locked fabric, the material can be block sampled and so intact samples that are effectively undisturbed can be tested.

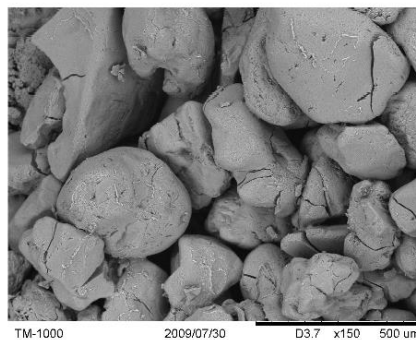


Figure 1: SEM image of Reigate Sand

The scanning electron microscope (SEM) micrograph of a carefully broken surface of the intact soil in Figure 1 shows the variety existing in the particle morphologies. The grain morphology varies from near-spherical grains to highly non-spherical grains with embayments. Figure 2 shows an optical microscope image of a thin section of Reigate sand under cross-polarised light that illustrates that the particles are essentially characterized by irregular and complex shapes, with occasional features such as long noses or necks. Cracks within the soil particles are evident in both the SEM and thin section images.

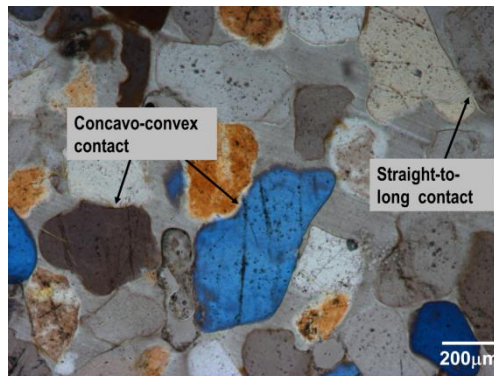


Figure 2 Optical microscope image of a thin section of Reigate Sand

### *Triaxial tests*

For triaxial testing small rectangular blocks of soil were extracted from the wooden boxes used to contain the intact soil during sampling and transportation (Figure 3). The small blocks were then trimmed in a hand lathe into cylinders (38mm in diameter by 76mm high). The samples were orientated with the long axis coinciding with the vertical in situ orientation. These samples had densities between  $1786\text{kg/m}^3$  and  $1796\text{kg/m}^3$ , with an average value of  $1790\text{kg/m}^3$ . The reconstituted samples were created using sand taken from the trimmings of the intact samples, any small clumps of material were greatly disaggregated. The cylindrical samples used in testing were created using a combination of pouring and tamping into a mould that was simultaneously tapped to induce vibration. These samples had a density range of  $1729\text{--}1.774\text{kg/m}^3$ , with an average value of  $1750\text{kg/m}^3$ , which is slightly lower than the density of the intact samples. While it would be interesting to compare relative densities, calculation of the relative density of the intact material is not possible due to the changes in morphology induced during reconstitution, which are evident in the data presented below.



Figure 3 Block of intact soil

The computer-controlled triaxial cell used to carry out the tests was a hydraulic stress path apparatus similar to that described by Bishop and Wesley (1975). The loading system was modified to ensure that the axial load was transmitted uniformly into the sample by using a half-ball connection between the top platen and the load cell, which minimized the development of non-uniformities during shearing. The samples were tested in a dry condition to facilitate impregnation with resin and the modifications to the triaxial apparatus

required for this resin impregnation are discussed in detail by Fonseca (2011). Since the samples were dry, the axial and radial strains were measured internally using LVDTs (Cuccovillo and Coop, 1997a) and the volumetric strains were calculated from these measurements.

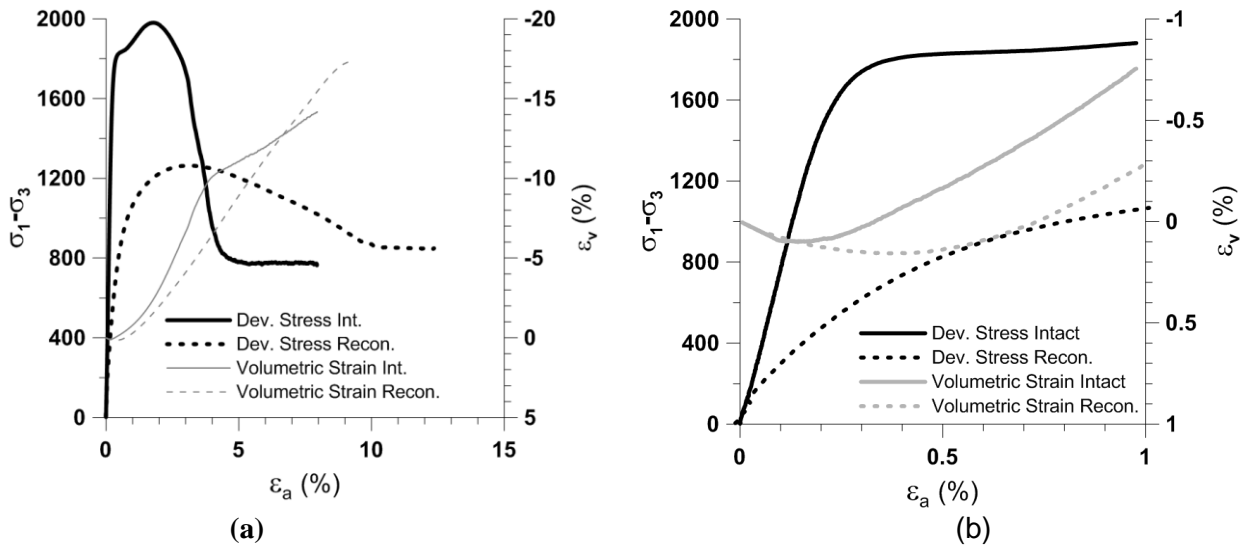


Figure 4 (a) Comparison of deviator stress and volumetric strain responses for representative intact and reconstituted samples (b) Plot of response up to a strain of  $\epsilon_a=1\%$  to highlight compressive responses at small strains

Thirteen triaxial tests were carried out, eight on intact samples and five on reconstituted samples, (see Table 1). Each sample was isotropically compressed to 300kPa at a rate of 50kPa/hour and then subjected to strain controlled compressive shearing at a rate of 1%/hour with a confining pressure of 300kPa. Both intact and reconstituted soil samples were impregnated prior to compression to obtain images of the material before shearing (stage 1.). The tests were stopped at three different stages during shearing: 2. at the onset of dilation, 3. once a shear band became visible, and 4. as the sample was approaching a critical state (albeit on a localized plane). At the end of each triaxial test the sample was impregnated with resin to enable specimens suitable for micro-CT scanning to be extracted, as discussed below. The stress-strain and volumetric strain responses are given in Figure 4(a), the response up to  $\epsilon_a=1\%$  is given in Figure 4(b) so that the onset of dilation in each sample can be clearly seen. While the two types of sample were made of the same source material and had very similar densities, their mechanical responses differed significantly. The intact soil showed a peak strength that is significantly higher than that of the reconstituted soil, and a correspondingly greater degree of strain-softening. The formation of a visible rupture occurred in the intact sample at an axial strain level of about 4% while in the reconstituted soil a visible shear band occurred at about 9% axial strain. Referring to Figure 4(b), at the onset of dilation stress ratios ( $q'/p'$ ) of were 1.7 and 1.35 were observed for the intact and reconstituted samples respectively. In the case of the intact soil, the peak stress ratio was mobilised well before the maximum dilation rate was achieved. Similar differences in response were observed by Cuccovillo and Coop (1997b) and Cresswell and Powrie (2004).

Table 1: Summary of the micro-CT data sets

Sample ref.	Loading stage	Sample diam. (mm)	Voxel size ( $\mu\text{m}$ )	No. of complete particles	Mean no. voxels per particle	$e_{\text{lab}}$	$e_{\text{CT}}$
Int-1a	Prior to iso comp	5	5	1438	74 059	0.48	0.43
Int-1b	Prior to iso comp	6	4	2849	138 600	0.48	0.43
Int-2a	Onset of dilation	5	5	1930	55 936	0.46	0.44
Int-2b	Onset of dilation	5	5	1635	66 254	0.46	0.43
Int-3a	Emergence of visible shear band <sup>a</sup>	5	5	2574	40 513	0.63	0.52
Int-3b(sb)	Emergence of visible shear band <sup>b</sup>	5	5	1912	47 200	0.63	0.68
Int-4a	Approaching a critical state <sup>a</sup>	5	5	1598	61 486	0.67	0.56
Int-4b(sb)	Approaching a critical state <sup>b</sup>	6	4	3247	104 570	0.67	0.67
Rec-1a	Prior to iso comp	5	5	2513	39 893	0.49	0.55
Rec-1b	Prior to iso comp	6	3	2110	169 740	0.49	0.64
Rec-3a	Emergence of visible shear band <sup>c</sup>	5	5	2704	35 977	0.80	0.64
Rec-3b	Emergence of visible shear band <sup>c</sup>	5	5	3387	27 504	0.80	0.71
Rec-4(sb)	Approaching a critical state <sup>b</sup>	5	5	2591	35 070	0.74	0.68

<sup>a</sup> sample from outside the shear band

<sup>b</sup> sample include a significant part of the shear band

<sup>c</sup> sample may include part of the shear band

### ***Sub-sampling for micro-CT scans***

When using CT to characterize a material, the sample size is roughly proportional to the image resolution and the sample must be entirely contained within the field of view. To achieve the resolution necessary to characterize the morphology of Reigate sand required specimens of 6mm diameter or less. While some researchers (e.g. Hall et al., 2010) have used miniature triaxial apparatuses in geomechanics micro-CT studies, in the current research we chose to use conventional high quality testing facilities, resin impregnate and then sub-sample specimens for subsequent micro-CT scanning. Prior studies that used resin impregnation to preserve sand fabric include Palmer and Barton (1986) and Jang et al. (1999). The most critical requirement for a resin is that it should not cause disturbance to the soil fabric, for example because of its viscosity or shrinkage during curing. The resin used was EPO-TEK 301 (by Epoxy Technology Inc.). EPO-TEK 301 is a two-part epoxy resin that cures at room temperature within about 12 hours after mixing and has a relatively low viscosity (100cps at 25°C) and was also used in previous studies using the impregnation of sands (e.g. Palmer and Barton, 1986 and Jang et al., 1999). Figure 5 shows the arrangement of the triaxial apparatus for resin impregnation. The sample disturbance due to resin impregnation in the

current study was minimal. The volumetric strains were monitored during the impregnation process and there was a maximum increase in specific volume of 0.008. Once the resin had hardened, 10mm long cylindrical sub-samples with diameters between 5 and 6mm were cored from the triaxial samples, the load stage and locations of which are noted in Table 1.

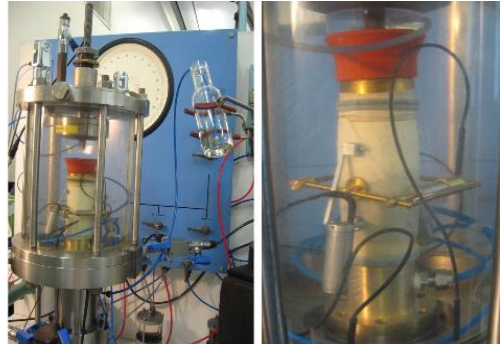


Figure 5 Resin Impregnation in the triaxial cell

***Image acquisition, processing and analysis***

Micro-CT scans generate three-dimensional images that map the variation of X-ray attenuation within objects; this attenuation is a function of the composition and density of the object and the beam energy. Each sample was scanned with a *Nanotom* (phoenix|x-ray, GE), rotating the sample 360° around its central axis between a X-ray source and a detector. When the beam passed through the specimen an X-ray a two-dimensional digital radiograph was recorded. A series of these images was acquired during a step-wise rotation of the object at pre-defined angular increments. These projections contain information on the position and density of the absorbing features within the sample. The data obtained is used for the numerical reconstruction of the final 3D image using a filtered back projection algorithm (Kak and Slaney, 2001). The voxel size of most of the images was 5µm, i.e. approximately  $0.015 \times d_{50}$ , where  $d_{50}$  is the median particle diameter as estimated from the sieve analysis. An example of a 3D output image is presented in Figure 6(a) and a cross-section through sample int-1a is given in Figure 6(b).

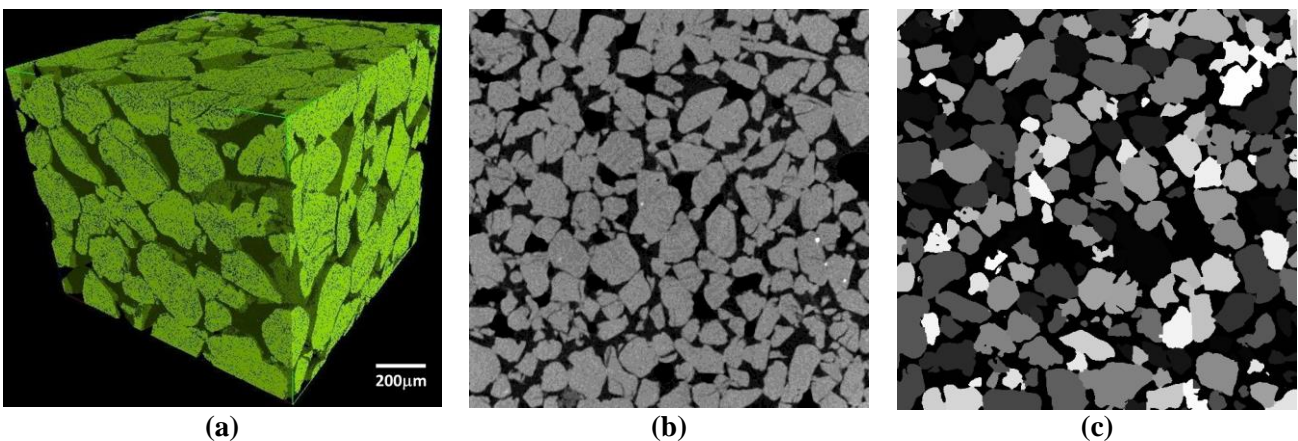


Figure 6 (a) 3D tomography image of Reigate Sand (Nanotom, resolution 0.8µm) (b) Section through data for sample Int-1a prior to filtering, thresholding or segmenting (c) Section through data for sample Int-1a following filtering, thresholding and watershed segmenting

The output of the micro-CT scan is a 3D map of the X-Ray attenuation. Further analysis of the data is needed to allow a quantitative description of the particle morphologies. The image analysis consisted of two main stages. Firstly the images were segmented or partitioned into regions or objects of interest, which in this case were the individual grains and the void space. In a second stage, measurements could then be obtained from the resulting images.

Thresholding segmentation was used to label each voxel as being either void space or solid particle. In the thresholding process the intensity of the attenuation value associated with each voxel is compared with a value that is chosen to divide particles from void space. To reduce the noise that typically is present in raw CT data and the images were pre-processed using a  $3 \times 3 \times 3$  median filter, a filter that avoids blurring of the image (Gonzalez and Woods, 2008). Choosing the threshold value is non-trivial and here the histogram of the intensity values was plotted and Gaussian curves were fitted to each of the two peaks of the histogram to determine the minimum point between them. The initial threshold value was verified using the method proposed by Otsu (1979), which divides the histogram into two classes and minimizes the intra-class variance between (algorithm implemented in ImageJ (Rasband, 1997-2011)). Alternative methods of thresholding have been proposed for granular materials, e.g. Chevalier and Otani (2011).

Figure 7 gives representative sectional binary images for an intact sample (Int-1a) and a reconstituted sample (Rec-1a) prior to loading. Qualitatively differences in the particle morphologies can be seen, there are smaller particles in the reconstituted sample and cracks are evident in a few of the particles in the intact sample. By identifying the voxels associated with each particle these differences could be quantified. This task was complicated by the fact that many of the particles were, often with extended contacts because of the locked fabric in the intact sample, refer to (Figure 7(a)). Particle segmentation was achieved using a morphological watershed algorithm, as proposed by Beucher and Lantuejoul (1979). The algorithm uses the principles that are used to identify catchment basins in hydrology and each particle is analogous to a single catchment basin. Firstly a distance map giving the distance of each particle voxel to the nearest void voxel was created and the watershed algorithm was applied to the inverse of this distance map. Individual particles were defined as the set of voxels whose path of steepest descent terminates at the same local minimum in the inverse distance map. The output of this process is an image in which different features are associated with different integers, i.e. the voxels representing the background or void space have a value of 0 and each particle voxel was assigned an index corresponding to an individual particle reference number. For each scan, the data was stored as a 3D matrix where each voxel is represented by an element of the matrix. A representative cross-sectional image of a segmented sample (sample Int-1a is illustrated in Figure 6(c)). Full details of the algorithm used here can be found in Atwood et al. (2004) and Gonzalez and Woods (2008).

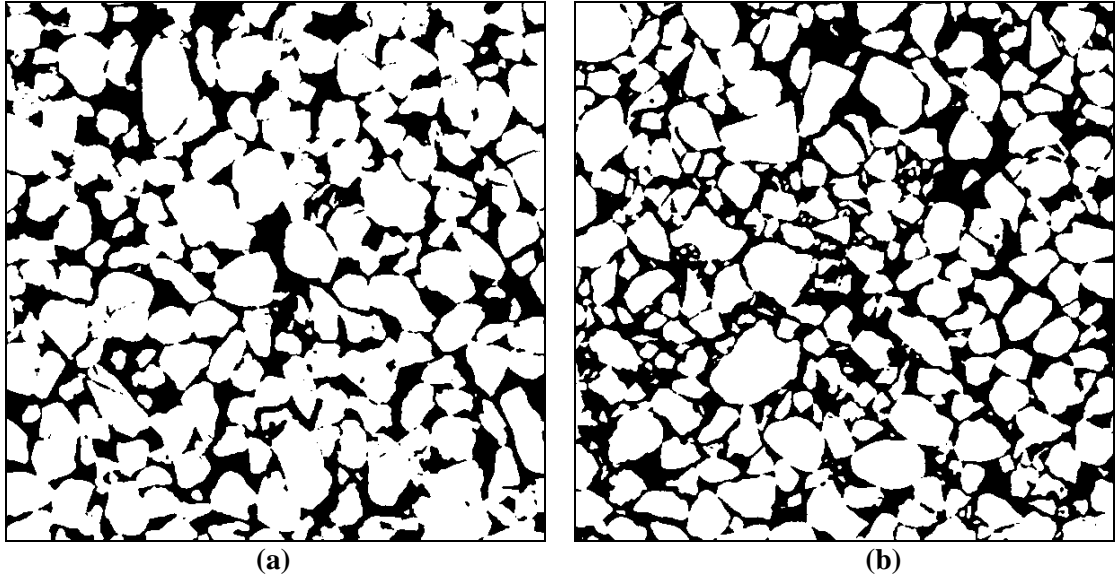


Figure 7 Representative cross-sectional binary images of thresholded intact and reconstituted samples prior to loading (a) Sample Int-1a (b) Sample Rec-1a

To identify the boundary voxels the intrinsic MATLAB function **bwperim** (Mathworkds, 2010) was applied to each individual particle. This considers a given voxel to be a perimeter voxel if it has a non-zero value and is connected to at least one zero-valued pixel. The associated search process considered a 6-connected neighbourhood. This level of connectivity was selected by considering an image of 555 $\mu\text{m}$  diameter precision microspheres. Using a connectivity of 6 the calculated surface areas differed from the analytical values by 15%; this error can be explained in part by small geometrical imperfections in the spheres and the “bumpy” nature of the reconstituted surface because the voxels have a finite size relative to the particle. When the order was increased to 18- and 26-connectivity, higher error values of 30% and 50% respectively were found.

Principal component analysis (PCA) was applied to determine the orientations of the major, minor and intermediate axes for each particle. The mathematics of the PCA method are outlined in Haralick and Shapiro (1992), it has been applied to analysis of tomographic references in other fields (e.g. Phillion et al. (2008) or Zhang et al. (2009)) and its application to soil particles is discussed in detail by Fonseca (2011). Knowing the principal axis orientations an orthogonal rotation was applied to the voxel coordinates to rotate each particle so that its principal axes of inertia were parallel to the Cartesian axes. The major ( $a$ ), intermediate ( $b$ ) and minor ( $c$ ) dimensions of the particle were calculated respectively as  $a = \max(\mathbf{x}^{rot}) - \min(\mathbf{x}^{rot})$ ,  $b = \max(\mathbf{y}^{rot}) - \min(\mathbf{y}^{rot})$  and  $c = \max(\mathbf{z}^{rot}) - \min(\mathbf{z}^{rot})$ , where  $\mathbf{x}^{rot}$ ,  $\mathbf{y}^{rot}$  and  $\mathbf{z}^{rot}$  are 1D arrays giving the particle’s voxel coordinates following rotation. The three principal lengths of each particle in microns were then obtained by multiplying the length given in voxels by the size of each voxel (resol). As the particles in the boundary of the image were not complete, only the inner particles of the image that did not touch the boundary were considered for morphological analysis. Table 1 summarizes the micro-CT data sets acquired for analysis in this study, giving information on the diameter and voxel size

(resolution) of each sample, number of particles and the comparison between the void ratio measurements using the sample weight ( $e_{lab}$ ) and using the micro-CT data ( $e_{CT}$ ).

## ***2D Morphology Analysis***

The 3D measurements of particle morphology were compared with 2D measurements obtained using the QICPIC apparatus (Sympatec, Germany). Details of the underlying technology are given by Altuhafi et al. (2011), Witt et al. (2004) and Sympatec (2008). In the current study a reconstituted sample of the soil was allowed to flow, at a controlled rate, between a laser and a high speed camera. The binary images captured by the camera images are then analysed by propriety software to obtain distributions of particle size and shape. As the pixel size for the dry dispersion unit is  $10\mu\text{m}$ , a rule of thumb is that particles smaller than 100 micron must be excluded from consideration. The analysis of the resulting images uses measures that are implemented in a number of imaging software packages (e.g. Axiovision (Carl-Zeiss-Micro Imaging 2007), ImageJ (Rasband, 1997-2011)), and consequently while the data considered in the current study were generated using the QICPIC apparatus, it is straightforward to apply the analysis approaches used to images of particles obtained using other methods.

## **RESULTS**

### ***Particle size distribution***

As discussed by Cavarretta (2010) when using image-based data, some consideration must be given as to what is meant by the size of an irregularly shaped particle. The Feret diameter ( $F$ ) is defined as the distance between two parallel tangents to the particle outline. The maximum and minimum Feret diameters are the largest and the smallest values of  $F$  for a given outline and these can be calculated from the 2D laser scanning (QICPIC) data ( $F_{min}^{LS}, F_{max}^{LS}$ ). The 3D analogues to these dimensions are the principal axes lengths, calculated as described above. The laser scanning system provides other measures of size, for example  $EQPC^{LS}$  is the diameter of a circle whose area equals the projected area of the particle. Alternative measures for use with 3D data sets that consider averaging of two or more measurements were proposed by Al-Raoush (2007) and Hasan and Alshibli (2010).

Figure 7 compares the particle size distribution data for the reconstituted material obtained using the micro-CT data, the QICPIC apparatus, and standard sieving. The match between the sieve data and the distribution of  $b$  values is very good. This provides a validation of the micro-CT data as it is the intermediate principal axis length that determines which sieve a given particle will pass through, assuming the energy imposed during sieving is sufficient for the particles to pass through the sieve with their major axes orientated vertically. The maximum and minimum principal axes lengths ( $a$  and  $c$ ) obtained from the micro-CT data bound all the data. The  $F_{max}^{LS}$  values closely approximate the  $a$  values, indicating that the QICPIC data can correctly identify the maximum particle dimension, but the  $F_{min}^{LS}$  values are larger than the  $c$  values; this can

be explained by the manner in which the QICPIC data is obtained, using 2D silhouette images of the particles falling under gravity; the value of  $F_{\min}^{LS}$  will only match the minimum particle dimension if the particle falls so that its intermediate axis is orthogonal to the camera lens. The average major axis length and the  $EQPC^{LS}$  values also give a close approximation to the sieve data. These observations may not, however, be applicable to all sands; Altuhafi et al. (2011) considered a number of sands and concluded that the  $F_{\min}^{LS}$  distribution values approximate sieve data more closely than the  $EQPC^{LS}$  data.

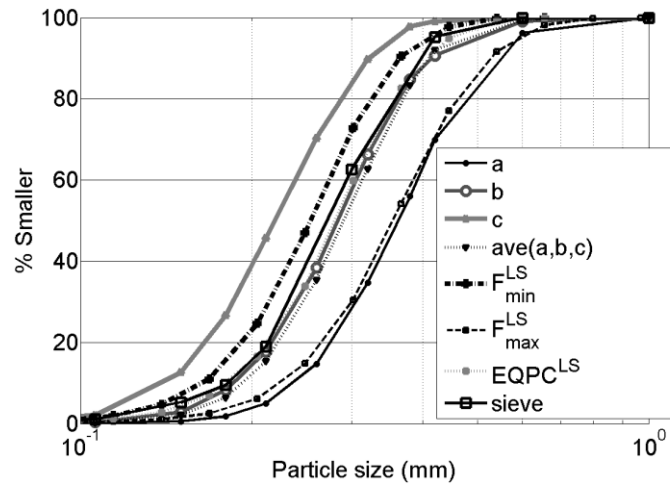


Figure 8: Comparison of particle size distribution of reconstituted sand quantified using various 2D and 3D measures

The intermediate principal axis length  $b$ , was used to compare the PSDs of the intact and reconstituted samples and examine the evolution of the PSDs during shearing. Comparing the data presented in Figures 8 and 9, there is a clear difference between the intact and reconstituted materials. For the reconstituted specimens that were scanned prior to loading (Rec-1a and Rec-1b), the micro-CT  $d_{50}$  value (measured by considering the intermediate axes lengths,  $b$ ) was  $284\mu\text{m}$  and the coefficient of uniformity ( $C_u$ ) was about 1.65. In contrast, for the intact specimens prior to loading (samples Int-1a and Int-1b) a significantly larger  $d_{50}$  value of  $324\mu\text{m}$  was obtained, coupled with a lower  $C_u$  (approx 1.53).

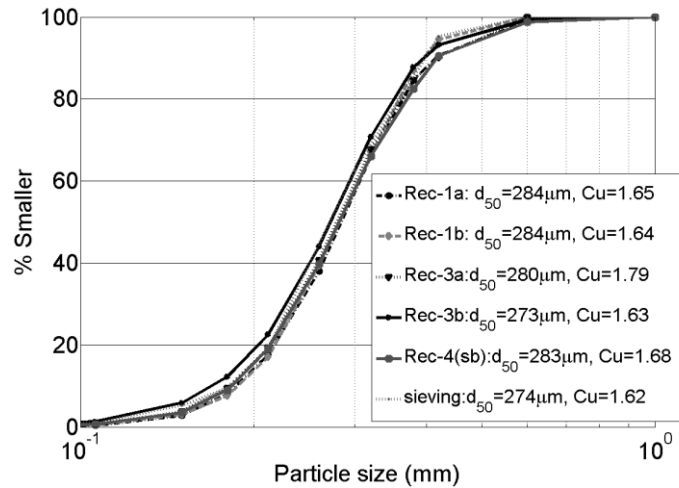


Figure 9 PSDs for the reconstituted samples

Further consideration of Figure 9 reveals that amongst some scatter in the data there is perhaps a general decrease in median particle diameter and an increase in Cu as shearing progresses to the onset of dilation (Int-2a and Int-2b;  $d_{50} \approx 306 \mu\text{m}$ ;  $\text{Cu} \approx 1.54$ ), the start of a visible shear band (Int-3a and Int-3b(sb);  $d_{50} \approx 283 \mu\text{m}$ ;  $\text{Cu} \approx 1.58$ ), and finally as the sample approaches a critical state (Int-4a and Int-4b(sb);  $d_{50} \approx 318 \mu\text{m}$ ;  $\text{Cu} \approx 1.62$ ). Samples Int-3b(sb) and Int-4b(sb) were taken so that they partially intercept the shear band, whereas Int-3a and Int-4a were taken from the same specimens but outside the shear bands. It is interesting that within the data scatter there is no significant difference in the PSDs for the samples taken from outside the shear band and the samples that partially contained the shear band.

The difference between the particle size distributions of the intact and reconstituted samples and the apparent evolution of the particle size distribution during shearing can be explained by the disintegration of the particles along the fissures observed in the SEM images and the micro-CT scans of the intact material (Figures 1, 2 and 6), which occurred both during shearing and during the reconstitution process. For this reason there is almost no change on the particle size distribution on the reconstituted soil in Figure 8. This difference in particle size distribution explains, in part, the difference in response between the intact and reconstituted samples. The lower  $d_{50}$  and the higher coefficient of uniformity of the reconstituted sample enabled samples with void ratios equivalent to the intact samples to be created without the need to form the characteristic locked fabric of the intact material.

### ***Particle shape***

Quantifying particle shape is non-trivial, as discussed by Cavarretta (2009). Traditionally geotechnical engineers have relied on qualitative measures, such as classifying particles as angular or rounded following Powers (1953) or comparing their particles with the chart provided by Krumbein and Sloss (1963). Digitized image data, such as the 3D data obtained in this study, allows quantitative measurements of particle shape to be made. While it is tempting, when armed with such data, to apply complex algorithms to describe

geometry, they are not always useful, as shown by Fonseca and O’Sullivan (2008). Here, relatively simple metrics were applied to assess whether there were any marked differences in the geometry of the intact and reconstituted samples and to evaluate whether the shape evolved noticeably during loading.

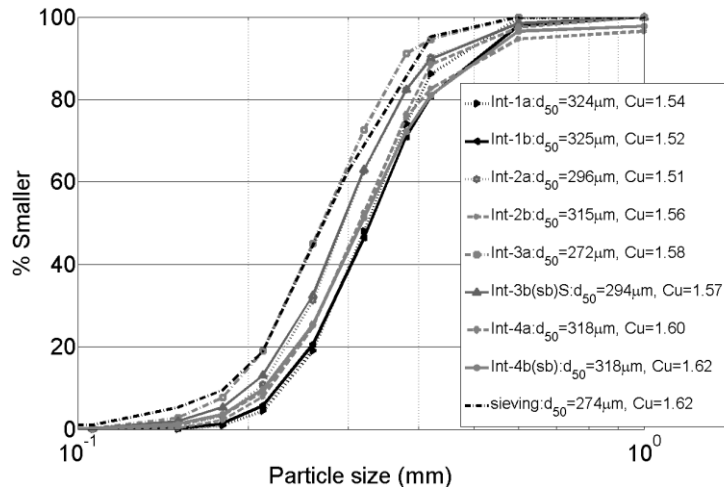


Figure 10 PSD for the intact samples

Table 2: Summary of morphology data

Sample ref.	$d_{50}$ ( $\mu\text{m}$ )	Cu	$FI_{50}$	$EI_{50}$	$S_{50}$	$CX_{50}$
Int-1a	324	1.54	0.793	0.792	0.918	0.805
Int-1b	325	1.52	0.794	0.790	0.892	
Int-2a	296	1.51	0.788	0.788	0.948	0.831
Int-2b	315	1.56	0.788	0.790	0.947	0.829
Int-3a	272	1.58	0.778	0.789	0.989	0.861
Int-3b(sb)	294	1.57	0.781	0.788	0.971	0.837
Int-4a	318	1.60	0.775	0.789	0.968	0.844
Int-4b(sb)	318	1.62	0.788	0.789	0.930	
Rec-1a	284	1.64	0.778	0.786	0.980	0.828
Rec-1b	284	1.65	0.769	0.783	0.958	
Rec-3a	280	1.74	0.770	0.784	0.991	0.850
Rec-3b	273	1.63	0.770	0.772	1.000	0.858
Rec-4(sb)	283	1.68	0.780	0.780	0.979	0.829

The first shape characteristic considered from the micro-CT data was the aspect ratio. As the data for each particle were 3D, two measures of aspect ratio were applicable, these are the elongation index ( $EI$ ) and the flatness index ( $FI$ ), which are defined as  $EI=b/a$  and  $FI=c/a$  where  $a$ ,  $b$  and  $c$  are the principal axes lengths. Figures 10 and 11 give distributions of the  $EI$  and  $FI$  values respectively for representative intact and reconstituted samples. The median  $FI$  and  $EI$  values for all samples are listed in Table 2. In general there are only small differences between the median values and the distributions in both cases. The only consistent

observation that can be made is that the *EI*, and to a lesser extent the *FI* values, for the reconstituted samples are consistently slightly lower than those of the intact samples. This may be a consequence of the new fragments formed by detachment along the fissures in the particles being more elongated than the parent particles.

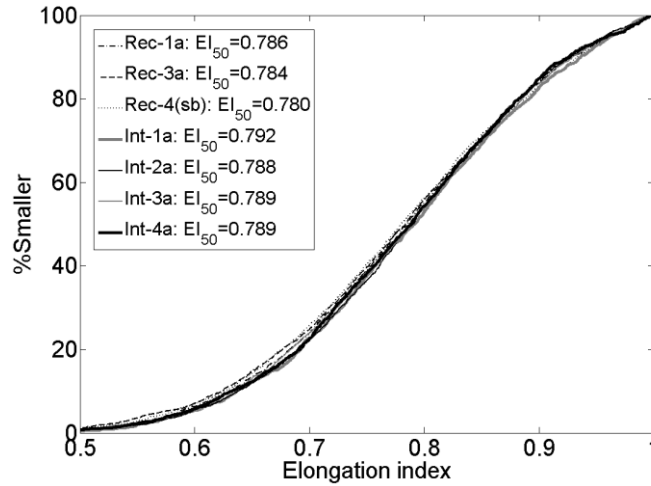


Figure 11 Elongation index data for representative intact and reconstituted samples

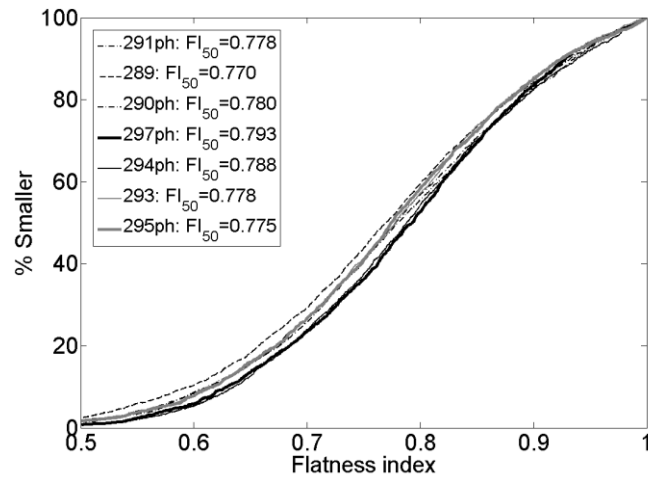


Figure 12 Flatness index data for representative intact and reconstituted samples

Figure 12 shows the flatness index plotted against the elongation index for one representative reconstituted sample following isotropic compression; similar data was obtained for other samples. The majority of the particles are located in zone II which according to Zingg (1935) classifies them as spheroids, i.e. the minor and intermediate axes are approximately equal in length. In Figure 13, the 3D aspect ratios are compared with the 2D values obtained using QICPIC. The 2D distribution does not correlate well with any of the 3D measures of aspect ratio and, as would be expected from geometrical considerations, the 2D data are intermediate between the *EI* and *FI* values obtained from the micro-CT data. Indeed it would be expected that the 2D data would lie between them.

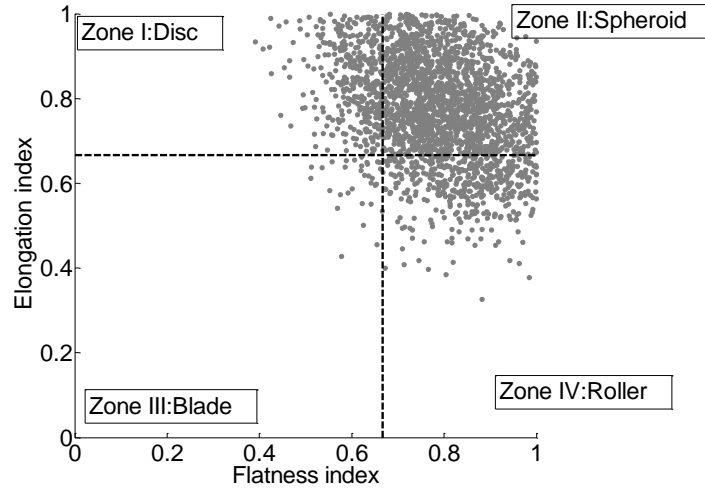


Figure 13 Elongation plotted against flatness for a representative reconstituted sample before shearing (Rec-1a), comparing with the Zingg (1935) shape classification

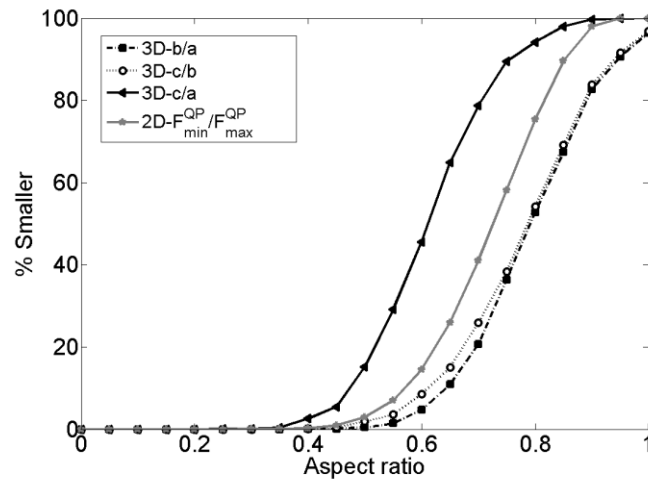


Figure 14 Aspect ratio comparison between 2D and 3D measurements (using reconstituted samples)

Sphericity describes how closely a particle resembles a sphere, or in other terms, it provides a measure of compactness. It was originally defined as  $SA_{sphere}/SA$ , where  $SA$  is the particle surface area and  $SA_{sphere}$  is the surface area of a sphere having the same volume as the particle (Wadell, 1932). Here the sphericity  $S$  was

calculated as  $S = \frac{\sqrt[3]{36\pi V_p^2}}{SA}$ , where  $V_p$  is the particle volume and  $SA$  is the surface area of the particle.

Sphericity distributions for representative intact and reconstituted samples are given in Figure 14. As noted above, the accuracy of the calculation of the sphericity is compromised by the error introduced by the finite size of the voxels; those particles whose sphericities exceed 1 have less than 2000 voxels (i.e. a diameter smaller than  $50\mu\text{m}$ ). It appears, however, that in general the reconstituted samples have higher sphericities than the intact samples. This can be explained by the likely fracture of particles along relatively narrow embayment or neck features, and such disintegration will result in the division of a single non-convex non-spherical particle into two more convex and more spherical particles. The higher sphericities of the reconstituted samples may also be related to the abundant small fragments covering only a small number of

voxels and consequently being associated with high sphericity values. Referring to Table 2, the sphericities of the intact samples tend to increase during shearing. These observations again indicate that the sharper corners of the particles are being broken off during shearing and in the reconstitution process.

Convexity is a measure of compactness of a particle and in three dimensions. It is defined as  $CX = \frac{V_P}{V_{CH}}$

where  $V_{CH}$  is the volume of the convex hull enclosing the sample. Distributions of convexity for representative samples are given in Figure 15. The intact sample has particles with complex shapes as embayments and long necks as observed in the microscope images of thin sections and this fact explains the lower convexity values of the intact sample prior to loading (Int-1). The breakage that occurs during reconstitution and shearing with the detachment of the small fragments contributes to the increase in compactness and consequently of convexity of the particles as observed for the intact sample after shearing Int-3 and the reconstituted samples Rec-1 to Rec-4. The shape parameters are not independent measures; there is a strong correlation between the sphericity and convexity values as is indicated in Figure 16(a) but poor correlation between both the flatness index and the elongation index and the sphericity as indicated in Figure 16(b).

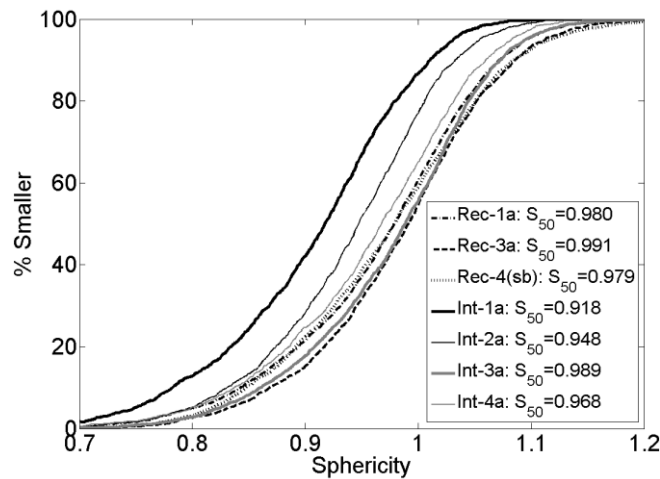


Figure 15 Sphericity index distributions for representative intact and reconstituted samples

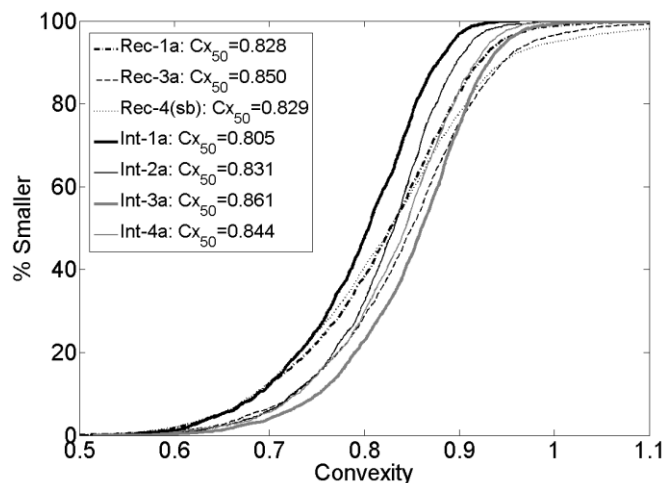


Figure 16 Convexity index distributions for representative intact and reconstituted samples

The 3D measures of sphericity and convexity are compared with the results obtained from the QICPIC 2D analyser obtained using the area of the binary images and shown in Figure 17 for the reconstituted sample prior to loading (Rec-1a). The 3D convexity values tend to be lower than the 2D values, while the 3D sphericity values tend to exceed the 2D values. In both cases the range or distribution of values is markedly higher for the 3D data. It is also worth noting that the QICPIC images have a pixel size of 10 microns compared to the voxel size of 5 microns used in the CT images.

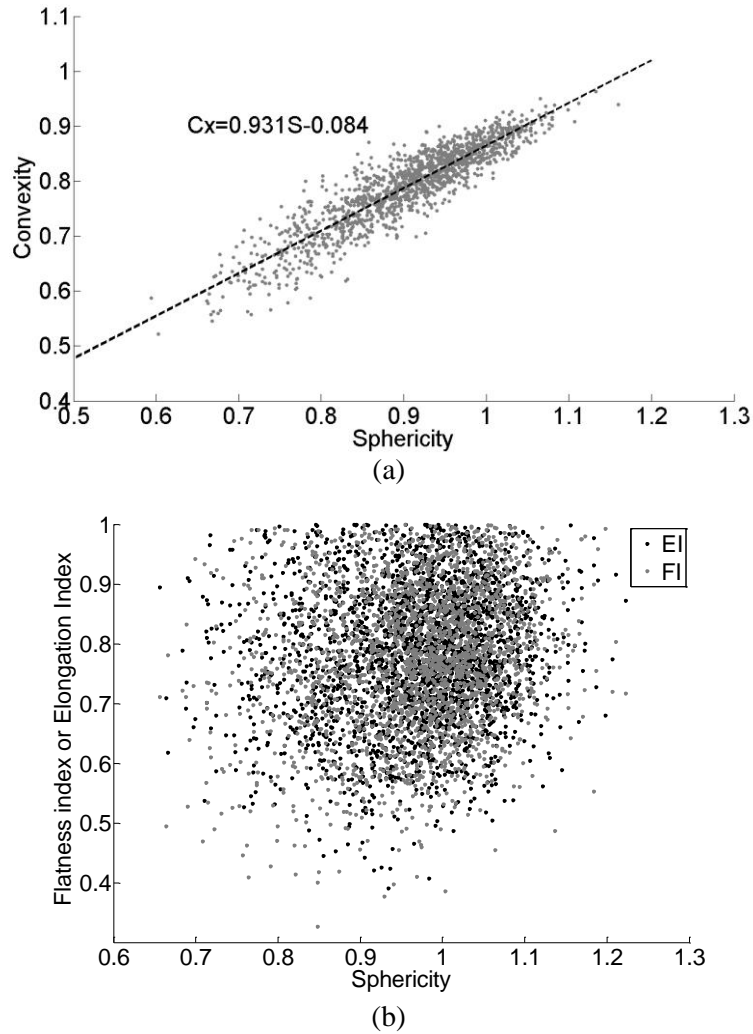


Figure 17 Correlations between shape metrics for reconstituted sample Rec-1a

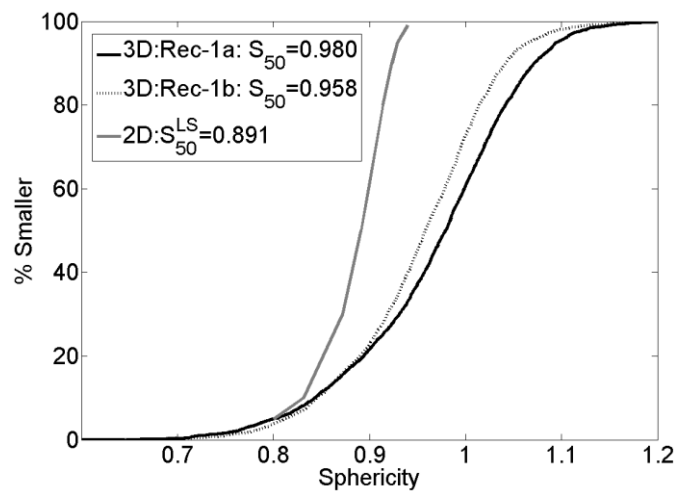
## CONCLUSIONS

The traditional means of assessing the effects of structure in soil mechanics has been to compare the behaviour of the intact soil with the same soil in a reconstituted state. However, in the case of the geologically old Reigate sand studied here the destructuration of the sand has been found to affect the grading of the material through breakage of grains along existing fissures during reconstitution. The observation of the change in grading during reconstitution of the intact soil indicates that fundamental differences exist between both materials and consequently different responses were to be expected between the intact and the reconstituted soil. A possible example can be the fact that Cuccovillo and Coop (1997) had found that the intact and reconstituted Greensand had different locations of the Critical State Lines in the

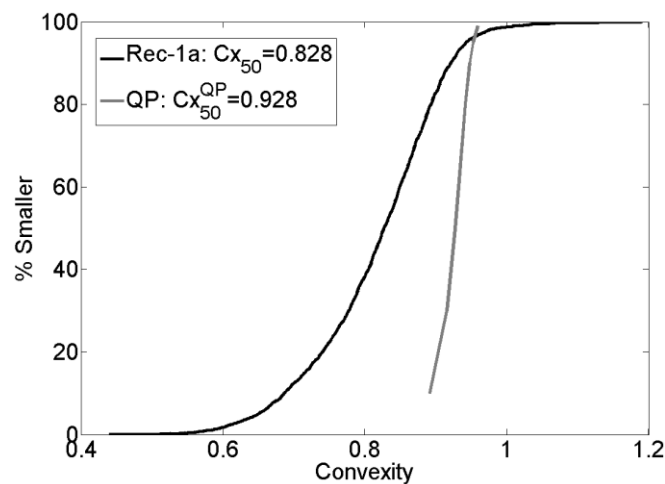
void ratio: log mean stress plane, although their samples were from a different location and were also lightly cemented.

Traditional methods of assessing grading such as sieving and laser diffraction techniques may not therefore be able to measure the operational grading of some intact sands, due to their invasive nature. As a consequence of the soil breakage, not only the size but also the shape of the grains differs between the intact and the reconstituted samples. As a consequence of the breakage the reconstituted samples have particles that are generally more elongated when compared with the particles of the intact samples. This highlights the fact that for some soils the traditional method of assessing the effects of structure by comparing the intact behaviour with that of the same soil when reconstituted may not be appropriate.

Calculations of particle size and shape made by analysis of 2D binary images of the particles differ noticeably from the 3D values when either the average values or the distribution of values are considered. While 2D data may be useful when comparing geometries of different sands, it cannot be used to reproduce accurately particle size and shape, for example for inclusion in a 3D discrete element model.



(a)



(b)

Figure 18 Comparison of 2D and 3D measures of sphericity and convexity

## ACKNOWLEDGEMENTS

The investigation presented in this paper were carried out under the financial support of a Portuguese Government Body, Fundação para a Ciência e a Tecnologia, as part of the PhD research of the first author.

The authors gratefully acknowledge the EPSRC (EP/F001452/1 & EP/I02249X/1) for funding. The authors are also grateful to GE Measurement & Control Solutions (Germany) for their support in the micro-CT imaging acquisition. The QICPIC apparatus was funded by EPSRC grant EP/F068778/1.

## REFERENCES

- Al-Raoush, R. (2007) Microstructure characterization of granular materials *Physica A* 377(2), 545-558.
- Altuhafi F., O'Sullivan, C. and Cavarretta, I. (2011) Analysis of an image based method for size and shape quantification of sand. Submitted to ASCE Journal of Geotechnical and Geoenvironmental Engineering September 2011
- Atwood, R. C., Jones, J. R., Lee, P.D. and Hench, L.L. (2004) Analysis of pore interconnectivity in bioactive glass foams using X-ray microtomography. *Scripta Materialia* 51, 1029-1033.
- Bauer, A., Verhulp, E., and Schoofs, S. (2004) Measuring local strains in sandstones under stress with micro-computed tomography in *Advances in X-ray Tomography for Geomaterials*, Desrues, Viggiani, Besuelle eds., ISTE, 2006.pp 247-254
- Beucher, S. and Lantuejoul, C. (1979) Use of watersheds in contour detection. *In Proc. Int. Workshop Image Process.* CCETT, Rennes, France.
- Bishop, A. W. and Wesley, L.D. (1975) A hydraulic apparatus for controlled stress path testing *Géotechnique* 25(4), 657-670.
- Carl-Zeiss-Micro Imaging (2007). Axiovision. Release 4.6.3 . Gottingen.
- Cavarretta, I. (2009) *The Influence of Particle Characteristics on the Engineering Behaviour of Granular Materials*, PhD Thesis, Dept. Civil and Environmental Engineering, Imperial College London.
- Chevalier, B. And Otani, J. (2011) Arching observation in three-dimensional trapdoor problem with x-ray CT and discrete element method *Soils and Foundations* 51(3) 459-469
- Clayton, C., M. Xu, and Bloodworth, A. (2006) A laboratory study of the development of earth pressures behind integral bridge abutments *Géotechnique* 56(8), 561-572
- Cresswell, A. and Powrie, W. (2004). Triaxial tests on an unbonded locked sand *Géotechnique* 54(2), 107-115.
- Cuccovillo, T. and Coop, M.R. (1997a). The measurement of local axial strains in triaxial tests using LVDTs. *Géotechnique*, 47, No.1, 167-171.
- Cuccovillo, T. and Coop, M.R. (1997b). Yielding and pre-failure deformation of structured sands. *Géotechnique* 47(3), 491-508.
- Desrues, J., Chambon, R., Mokni, M. and Mazerolle, F. (1996). Void Ratio evolution inside shear bands in triaxial sand specimens studies by computed tomography. *Géotechnique* 46(3), 529-546.
- Dusseault, M. B. and Morgenstern, N.R. (1979). Locked sands. *Q. J. Engng Geol.* 12, 117-131.
- Fonseca (2011) *The evolution of morphology and fabric of a sand during shearing* PhD Thesis, Imperial College London, University of London
- Fonseca, J. and O'Sullivan, C. (2008) A re-evaluation of the Fourier descriptor approach to quantifying sand particle geometry, 4th International Symposium on Deformation Characteristics of Geomaterials, IOS Press, 687-693
- Gonzalez, R. C. and Woods, R.E. (2008). *Digital Image Processing*. Prentice Hall.
- Guo, P. and Su, X. (2007). Shear strength, interparticle locking, and dilatancy of granular materials. *Canadian Geotechnical Journal* 44, 579-591.
- Hall, S., Bornert, M., Desrues, J., Pannier, Y., Lenoir, N., Viggiani, G. and Bésuelle P. (2010) Discrete and continuum analysis of localised deformation in sand using X-ray microCT and volumetric digital image correlation. *Géotechnique* 60(5), 315-322
- Hasan, A. and Alshibli, K. (2010). Experimental assessment of 3D particle-to-particle interaction within sheared sand using synchrotron microtomography. *Géotechnique* 60(5), 369-379.
- Haralik, R. and Shapiro, L. (1992) Computer and Robot Vision Addison Wesley Longman Publishing Co., Inc. Boston, MA, USA.

- Holtz, R. and Kovacs, W. (1981). *An Introduction to Geotechnical Engineering*. Prentice-Hall, Inc., Englewood Cliffs.
- Kak, A. and Slaney, M. (2001). *Principles of Computerized Tomographic Imaging*. SIAM, New York.
- Jang, D.-J., Frost, J. D., and Park, J.-Y. (1999). Preparation of Epoxy Impregnated Sand Coupons for Image Analysis. *Geotechnical Testing Journal* 22(2), 147-158.
- Kézdi, Á. (1979) *Soil physics: Selected topics.*, Elsevier.
- Kenney, TC and Lau, D. (1985) Internal stability of granular filters *Canadian Geotechnical Journal*, 22, 215-225.
- Krumbein, W.C. and Sloss, L.L. (1963) *Stratigraphy and Sedimentation* 2<sup>nd</sup> Ed, Freeman and Company, San Francisco.
- Mathworks (2010) MATLAB Version 7
- Miura, K., K. Maeda, Furukawa, M., and Toki, S. (1997). Physical characteristics of sand with different primary properties. *Soils and Foundations* 37(3), 53-64.
- O'Sullivan, C. (2011). *Particulate Discrete Element Modelling: A Geomechanics Perspective*. Taylor and Francis.
- Palmer, S. M. and Barton, M. E. (1986) Avoiding microfabric disruption during the impregnation of friable, uncemented sands with dyed epoxy *Journal of Sedimentary Petrology* 56 (4), 556-557.
- Phillion, A.B., Lee, P.D., Maire E. and Cockcroft, S.L. (2008) Quantitative assessment of deformation-induced damage in a semi-solid aluminum alloy via x-ray micro tomography, *Met. Trans., A* 39A(10), 2459-2469.
- Powers, M. C. (1953) A New Roundness Scale for Sedimentary Particles. *Journal of Sedimentary Research* 23(2) 117-119
- Rasband, W.S. (1997-2011) ImageJ, U. S. National Institutes of Health, Bethesda, Maryland, USA, <http://imagej.nih.gov/ij/>.
- Rothenburg, L. and Bathurst, R. J. (1992). Micromechanical features of granular assemblies with planar elliptical particles *Géotechnique* 42 (1), 79-95.
- Santamarina, J. and Cho, G. (2004) Soil Behavior: The Role of Particle Shape *In Proc. Skempton Conf., London*.
- Sympatec (2008). Windox - Operating Instructions Release 5.4.1.0 . Clausthal-Zellerfeld.
- Wadell, H. (1932). Volume, shape and roundness of rock particles. *J. Geol.* 40, 443-451.
- White, D.J. (2003) PSD measurement using the single particle optical sizing (SPOS) method. *Géotechnique* 53(3) 317-326
- Witt, W., Köhler U. and List, J. (2004) Direct Imaging of Very Fast Particles Opens the Application of the Powerful (Dry) Dispersion for Size and Shape Characterization. *Proceedings of PARTEC 2004, Nürnberg* (CD Proceedings).
- Yamamuro, J. and Wood, F. (2004) Effect of depositional method on the undrained behavior and microstructure of sand with silt. *Soil Dynamics and Earthquake Engineering* 24, 751-760.
- Zhang, Q., Lee, P.D., Singh, R., Wua, G., and Lindley, T.C. (2009) Micro-CT characterization of structural features and deformation behavior of fly ash/aluminum syntactic foam. *Acta Mat.* 57(10), 3003-3011.
- Zingg, T. (1935). Beitrag zur Schotteranalyse. *Schweizer Mineralogische Petrographologische Mitteilungen* 15, 52-56.